Magnetic Ground State Stabilized by Three-Site Interactions: Fe/Rh(111)

Andreas Krönlein,[1] Martin Schmitt,[1] Markus Hoffmann,[2] Jeannette Kemmer,[1] Nicolai Seubert,[1] Matthias Vogt,[1] Julia Küspert,[1] Markus Böhme,[1] Bandar Alonazi,[3] Jens Kügel,[1] Hamad A. Albrithen,[4,3,1] Matthias Bode,[1,5] Gustav Bihlmayer,[2] and Stefan Blügel[2]

[1]*Physikalisches Institut, Lehrstuhl für Experimentelle Physik 2, Universität Würzburg, Am Hubland, 97074 Würzburg, Germany*
[2]*Peter Grünberg Institut and Institute for Advanced Simulation, Forschungszentrum Jülich und JARA, 52425 Jülich, Germany*
[3]*National Center for Nanotechnology, King Abdulaziz City for Science and Technology, 11442 Riyadh, Saudi Arabia*
[4]*Physics and Astronomy Department and KAIN, King Saudi University, 11451 Riyadh, Saudi Arabia*
[5]*Wilhelm Conrad Röntgen-Research Center for Complex Material Systems (RCCM), Universität Würzburg, Am Hubland, D-97074 Würzburg, Germany*

(Received 10 November 2017; revised manuscript received 6 March 2018; published 14 May 2018)

We report the direct observation of a theoretically predicted magnetic ground state in a monolayer Fe on Rh(111), which is referred to as an up-up-down-down (↑↑↓↓) double-row-wise antiferromagnetic spin structure, using spin-polarized scanning tunneling microscopy. This exotic phase, which exists in three orientational domains, is revealed by experiments with magnetic probe tips performed in external magnetic fields. It is shown that a hitherto unconsidered four-spin–three-site beyond-Heisenberg interaction distinctly contributes to the spin coupling of atoms with $S \geq 1$ spins. The observation of the ↑↑↓↓ order substantiates the presence of higher-order, in particular, three-site interactions, in thin magnetic films of itinerant magnets.

DOI: 10.1103/PhysRevLett.120.207202

Magnetic interactions have captivated generations of physicists because of the diversity of their physical origins, the emergence of a vast spectrum of magnetic structures and phases on different length scales resulting from their competition, and, subsequently, the many interesting physical phenomena that are arising from those magnetic structures. Topological magnetization solitons such as chiral Skyrmions [1–3] are timely examples of intensively investigated complex magnetic structures with a large spectrum of exotic properties, interesting for basic research as well as relevant for applications [4]. Chiral Skyrmions result from a competition between the Heisenberg and the Dzyaloshinskii-Moriya interaction (DMI), the latter arising in lattices with broken inversion symmetry and spin-orbit interaction. In this context, itinerant magnets play an important role, as the itinerant electrons give rise to these complex magnetic structures, which, in turn, give rise to interesting transport phenomena.

Skyrmions in thin films and heterostructures stabilized by structural inversion asymmetry due to the presence of interfaces enjoy increased attention due to the compatibility with spintronics. Among those, the system Fe/Ir(111) [3] stands out, as it does not host single Skyrmions in an applied magnetic field but a square lattice ground state of nano-Skyrmions even without a field. A detailed analysis [3] discloses the four-spin–four-site cyclic ring exchange [5,6], a beyond-Heisenberg exchange interaction, as the origin of the stability of the square lattice. This is surprising, as so far the biquadratic (four-spin–two-site) exchange was the most commonly considered beyond-Heisenberg contribution of Fe, for example, noticeable as a small contribution to the temperature-dependent bulk spin wave spectrum [7].

In general, four-spin interactions are of great interest, because in the micromagnetic limit, applicable to slowly varying spin textures $\mathbf{S}(\mathbf{r})$, they resort to an energy functional $E_2 = F/2 \int d\mathbf{r}[\nabla^2\mathbf{S}(\mathbf{r})]^2$ with fourth-order terms in gradients of $\mathbf{S}$ of length $S = 1$. Together with the corresponding functional E_1 of the isotropic bilinear Heisenberg model, the magnetism is described by an energy functional $E = 1/2 \int d\mathbf{r}\{A[\nabla\mathbf{S}(\mathbf{r})]^2 + F[\nabla^2\mathbf{S}(\mathbf{r})]^2\}$, a form analogous to the original Skyrme model [8], stabilizing nonchiral Skyrmions without DMI if the spin stiffness A and the fourth-order strength F are in the right parameter range [9].

This motivates the investigation of an Fe monolayer on Rh(111), isoelectronic and isostructural to Fe/Ir(111), but with Rh having a much smaller spin-orbit interaction than Ir and thus a negligible DMI, unmasking the beyond-Heisenberg interactions. In a search for beyond-Heisenberg interactions, detailed first-principles investigations based on the density-functional theory [10] predicted a novel two-dimensional magnetic ground state structure for Fe/Rh(111): a lattice-commensurate double-row-wise antiferromagnetic (↑↑↓↓) order along the $\langle 1\bar{1}0\rangle$ direction with a periodicity of four atomic rows [cf. Fig. 1(a)]. This so-called $2Q$ state can be understood as a superposition of two particular spin spirals with opposite wave vectors $q = \pm\frac{1}{2}\overline{\Gamma M}$ in the two-dimensional Brillouin zone (2DBZ) [cf. Fig. 1(c)]. In general, the conditions for such superpositions are met only for a few special wave vectors across

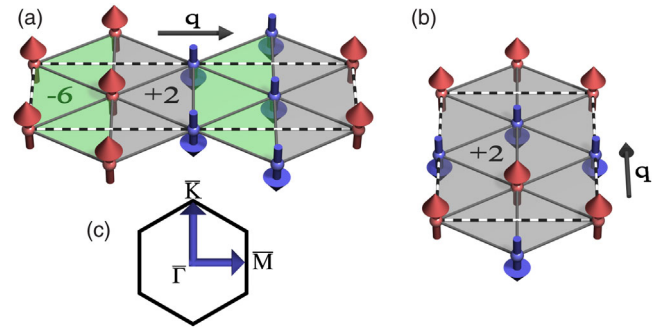

FIG. 1. Magnetic order of the $2Q$ spin spirals with (a) $q = M/2$ and (b) $q = 3K/4$. In the green shaded triangles, the four-spin–three-site interaction contributes by an energy of $-6Y_1$ and in the gray shaded triangles by $+2Y_1$, where Y_1 is the strength of the interaction in the nearest-neighbor approximation; see Eqs. (2) and (3). Unit cells are indicated by dashed lines. The Brillouin zone is shown in (c).

the 2DBZ. Along the symmetry line $\overline{M\Gamma M}$, there are exactly those two q vectors, which encode the commensurability of the structure. This magnetic structure is surprising, as neither the formation of a commensurate magnetic structure along $\langle 1\bar{1}0\rangle$ beyond period 2 nor the formation of the $2Q$ state can be explained by the Heisenberg model alone. Its bilinear form neither facilitates the energy gain to couple $1Q$- to multi-Q states nor does it provide a mechanism to stabilize collinear magnetic state for wave vectors between the $\bar{\Gamma}$ and $\bar{M}$ points. The $\uparrow\uparrow\downarrow\downarrow$ order was first discovered for nuclear spins in solid ^{3}He [11,12] and later in some perovskites [13] and explained by the cyclic ring or biquadratic exchange, respectively. This is different for Fe/Rh(111), where a detailed analysis [10] revealed the surprising fact that neither one can consistently explain the $\uparrow\uparrow\downarrow\downarrow$ structure.

In this Letter, (i) we validate and confirm the first-principles prediction by state-of-the-art spin-polarized-(SP-)STM measurements. Furthermore, (ii) based on a systematic derivation of all four-spin interactions obtained by a multiband Hubbard model [14] up to the fourth-order perturbation theory in the hopping parameter t versus Coulomb interaction U, t^4/U^3, we argue that the origin of this spin structure is a missing four-spin–three-site interaction [15]. Note that in the past this interaction and variants of it were referred to as a three-spin interaction, a nomenclature that has recently drawn criticism, as the interaction indicates a lack of time-inversion symmetry. In Ref. [14], we show that the four-spin–three-site interaction is zero for $S = 1/2$ systems and thus frequently ignored. On the other hand, the magnetic moment of Fe/Rh(111) is about $2.9\mu_B$; i.e., the magnetic spin-moment of Fe is $S \approx 3/2$, and this interaction term now becomes important.

Clean Rh(111) was prepared similarly to Rh(001) [16,17]. Fe films were deposited from e-beam evaporators at $p < 3 \times 10^{-10}$ mbar with the substrate held at

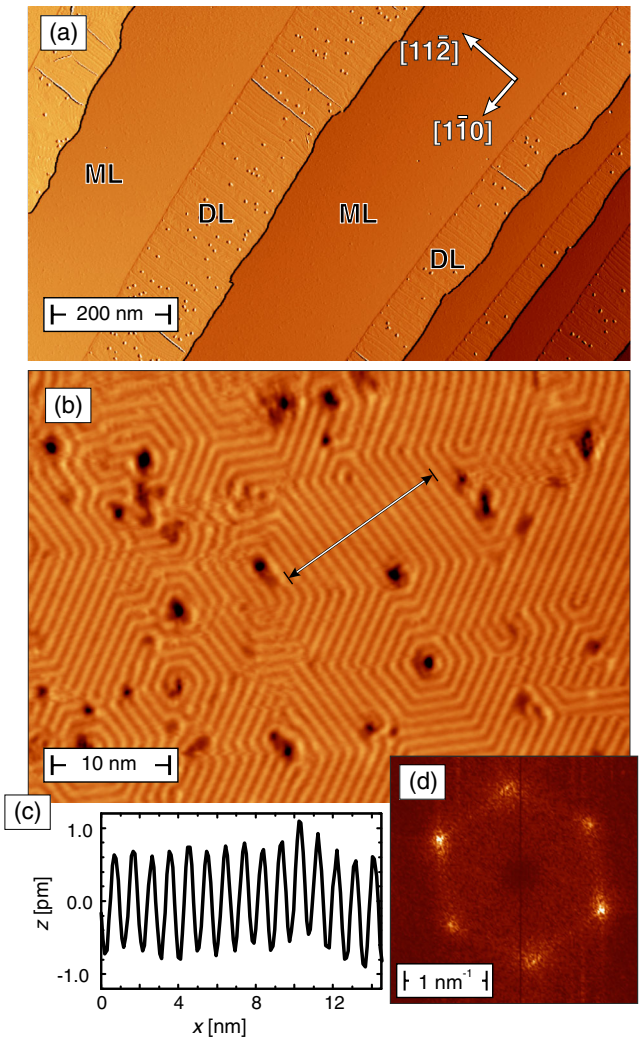

FIG. 2. (a) Topography of 1.3 AL Fe/Rh(111) (scan parameters $U = +1$ V and $I = 300$ pA) with alternating monolayer (ML) and double-layer (DL) Fe coverage. (b) Higher-magnification SP-STM image of the ML showing stripes along the $\langle 1\bar{1}0\rangle$ directions of the substrate ($U = +0.3$ V and $I = 1$ nA). (c) Averaged line profile taken along the arrow. The periodicity between the stripes amounts to (1.0 ± 0.1) nm with a corrugation of (1.4 ± 0.1) pm. (d) Fourier transformation of (b).

$T_S = (500 \pm 10)$ K. We used two homebuilt low-temperature STMs ($T \approx 5$ K), one of which is equipped with a superconducting magnet with a maximal magnetic field $\mu_0 H = 3$ T oriented along the sample's surface normal. Topographic images were obtained in the constant-current mode with the bias voltage U applied to the sample. We used electrochemically etched W tips, which were flashed by electron bombardment and gently dipped into Fe/Rh(111) for SP-STM experiments [18].

Figure 2(a) shows an overview image ($1\ \mu\text{m} \times 0.6\ \mu\text{m}$) of 1.3 AL Fe/Rh(111). Fe monolayer (ML) and double-layer (DL) regions are labeled correspondingly. Whereas the ML appears to be flat on the scale of this image, various dislocation structures can be recognized on the DL,

strikingly similar to Fe DL films grown on Ir(111) [19]. Since we will focus on the ML here, details of the DL are irrelevant and will not be discussed any further.

At a higher magnification, it becomes obvious that constant-current SP-STM images taken on ML regions of Fe/Rh(111) are not featureless but exhibit stripes [see Fig. 2(b)], which are oriented along the $\langle 1\bar{1}0\rangle$ directions and tend to be circularly arranged around occasional surface defects. An averaged line profile taken along the arrow is displayed in Fig. 2(c). It reveals a stripe periodicity of (1.0 ± 0.1) nm, in good agreement with the value of 0.931 nm expected for the $\uparrow\uparrow\downarrow\downarrow$ spin structure. Correspondingly, the Fourier transformation of the STM image shown in Fig. 2(b) leads to six spots at $k = 1/\lambda = (1.0 \pm 0.1)$ nm^{-1} [see Fig. 2(d)].

Before we present field-dependent data, it is worthwhile to consider what contrasts can be expected as the SP-STM setup is exposed to an external magnetic field. Four scenarios are sketched in Figs. 3(a)–3(d), all starting with the same domain structure and the same out-of-plane sensitive tip in the left column. Red and blue stripes represent the SP-STM signal obtained from $\uparrow\uparrow$ and $\downarrow\downarrow$ double rows, respectively, which coexist in three domains, $A/B/A$. If both the magnetic sample and the SP-STM tip remain unchanged upon field application, one will obtain the same SP-STM image as before [Fig. 3(a), middle column], and the difference between the two images will be zero. This is indicated by gray stripes in the right column in Fig. 3(a). Although the compensated $\uparrow\uparrow\downarrow\downarrow$ spin structure should, in principle, lead to a vanishing Zeeman energy if integrated over a sufficiently large defect-free surface area, we will see later on that the termination points of the $\uparrow\uparrow$ and $\downarrow\downarrow$ double rows often move if exposed to an external field, an effect we ascribe to the existence of uncompensated spins at domain boundaries. This situation is sketched in Fig. 3(b), where the two A domains merge and grow at the expense of B, resulting in a difference image with a characteristic hexagonal point lattice (right panel). Figure 3(c) exemplifies the impact of a domain which switches from $\uparrow\uparrow\downarrow\downarrow$ (B) to $\downarrow\downarrow\uparrow\uparrow$ (B^-) leading to an enhanced contrast at domain B (right column). Only if the tip reverses its magnetization direction but the sample's spin structure remains unchanged can we expect a difference image with a globally enhanced contrast [Fig. 3(d)].

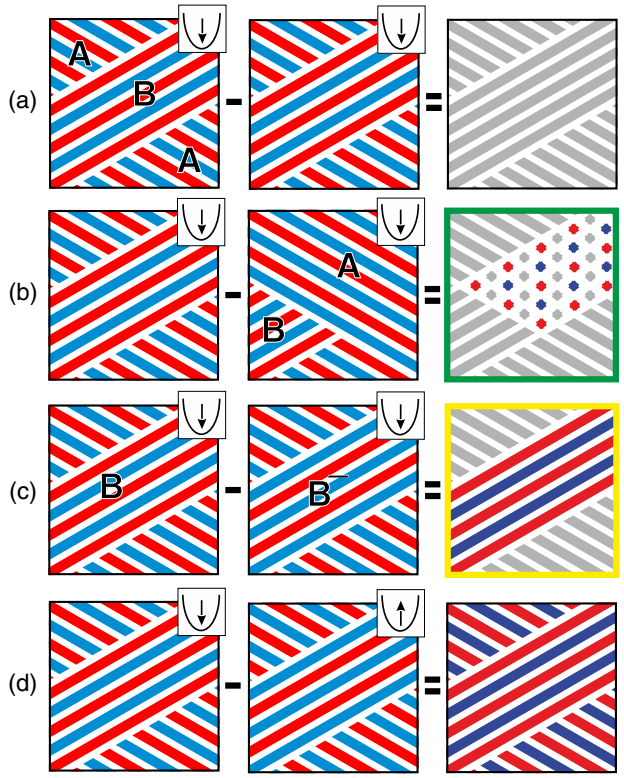

FIG. 3. Schematic representation of SP-STM contrasts expected for $\uparrow\uparrow$ (red) and $\downarrow\downarrow$ (blue) double rows. The tip is indicated in the upper right of each panel. The left (center) column shows the situation before (after) the application of a magnetic field. The right column is their difference image. (a) The domains remain unchanged; the difference image is featureless (gray). (b) One domain grows at the expense of another domain. (c) Reversal of domain B to B^-, leading to an enhanced line contrast. (d) Reversal of the SP-STM tip leading to a global enhancement.

Figure 4 shows SP-STM images of the Fe ML on Rh(111) measured at (a) $\mu H = 2.2$, (b) 2.4, and (c) 2.6 T. These data are only an excerpt of a complete hysteresis measured by sweeping the magnetic field between ± 2.6 T [20]. As indicated by a blue arrow pointing to a holelike defect, all data have been measured at the same position. Some characteristic regions which exhibit a behavior similar to what was schematically presented in Figs. 3(b) and 3(c) are highlighted by ellipses in Fig. 4. Whereas the overwhelming surface fraction of the difference image presented in Fig. 4(d) shows no clear contrast, thereby indicating that both the SP-STM tip and the sample magnetization remained unchanged when increasing the magnetic field from 2.2 to 2.4 T, it can easily be recognized that the orientation of the stripes in the green and red ellipse switched. In agreement with our expectations from Fig. 3(b), this leads to a hexagonal point lattice in the difference image [Fig. 4(d)]. In contrast, the region within the yellow ellipse exhibits a stripe pattern in Fig. 4(d), indicating an $\uparrow\uparrow\downarrow\downarrow$ to $\downarrow\downarrow\uparrow\uparrow$ reversal. Note that the contrast in Figs. 4(d) and 4(e) is about twice as strong as in Figs. 4(a)–4(c), in agreement with our expectations.

As the field is increased to $\mu H = 2.6$ T, a more general change can be observed. In contrast to Fig. 4(d), where only local contrasts were observed, the difference image in Fig. 4(e) shows a rather strong global stripe contrast. As pointed out in the context of Fig. 3(d), this indicates a magnetization reversal of the out-of-plane sensitive tip. Indeed, a corresponding behavior could also be observed at negative fields between -2.4 and -2.6 T [20]. This observation unambiguously proves the magnetic origin of the observed stripe contrast. We note that we

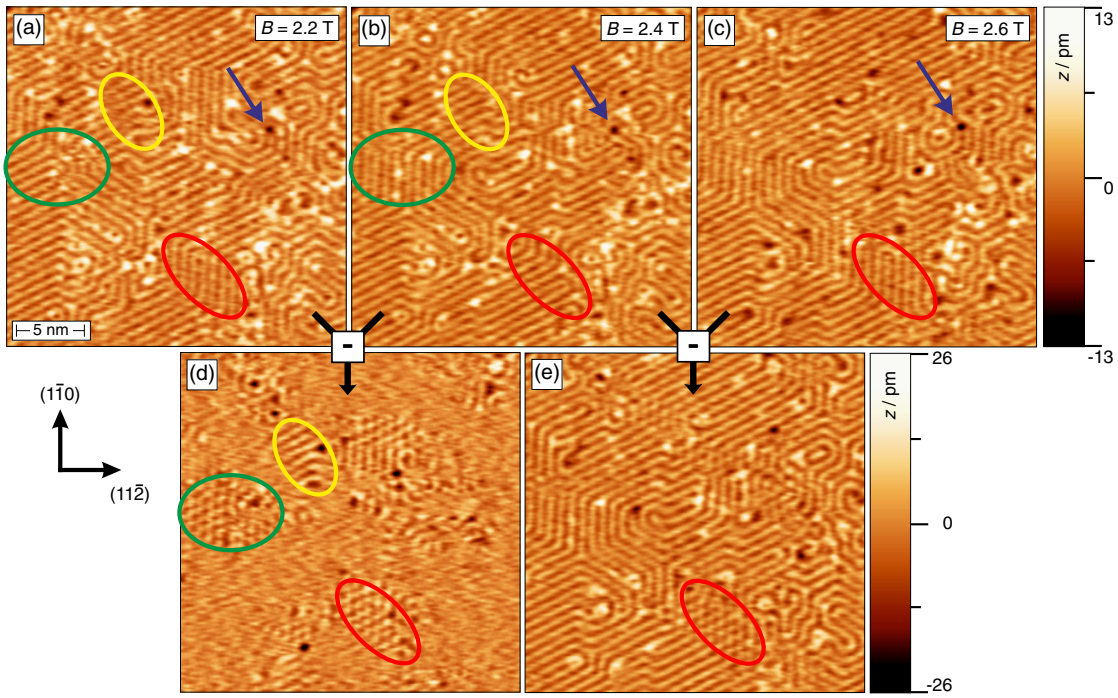

FIG. 4. (a)–(c) SP-STM data of an Fe monolayer on Rh(111) exhibiting the ↑↑↓↓ spin structure at external fields $\mu H = 2.2$, 2.4, and 2.6 T, respectively. (d),(e) Difference of the respective data sets. A global corrugation reversal occurs between 2.4 and 2.6 T, indicating tip magnetization reversal and unambiguously proving the magnetic origin of the stripe pattern. Scan parameters $U = +50$ mV and $I = 0.5$ nA.

could not detect any magnetic contrasts in experiments performed with in-plane sensitive Fe tips [20], providing further evidence against a spin spiral state and confirming a collinear ↑↑↓↓ spin structure.

We can now return to a more detailed analysis of the interactions that stabilize this unusual spin structure. In an extended Heisenberg Hamiltonian, which includes biquadratic (B) and cyclic four-spin interactions (K) within the nearest-neighbor approximation (indicated by subscript 1), the energy difference between the single- and double-Q states for a hexagonal lattice and $q = \pm\frac{1}{2}\overline{\Gamma M}$ amounts to

$$E_{2Q} - E_{1Q} = 4(2K_1 - B_1). \tag{1}$$

This energy difference was found by Al-Zubi, Bihlmayer, and Blügel [10] to be −29 meV/atom, a surprisingly large energy caused by higher-order interactions. On the other hand, it is also possible to form a $2Q$ structure from two spin spirals with $q = \pm\frac{3}{4}\overline{\Gamma K}$ [cf. Fig. 1(b)]. In this case, the energy difference is also given by Eq. (1) but amounts to +3 meV/atom, inconsistent with the previous result. Obviously, a term is missing in Eq. (1) which stabilizes the experimentally found $2Q_{\overline{\Gamma M}}$ (or ↑↑↓↓) spin structure.

Based on our recent analysis of higher-order spin interactions [14], we can demonstrate that the apparent discrepancy is resolved by including a four-spin–three-site interaction. The key point is a missing term to the spin-lattice Hamiltonian describing the extended Heisenberg model of classical spins S derived of the form

$$H_3 = -2\sum_{\langle ijk\rangle} Y_{ijk}[(\mathbf{S}_i\cdot\mathbf{S}_j)(\mathbf{S}_j\cdot\mathbf{S}_k) + (\mathbf{S}_j\cdot\mathbf{S}_k)(\mathbf{S}_k\cdot\mathbf{S}_i) + (\mathbf{S}_k\cdot\mathbf{S}_i)(\mathbf{S}_i\cdot\mathbf{S}_j)], \tag{2}$$

where the sum runs over all nearest-neighbor sites i, j, and k. Like the biquadratic interaction, this term arises from the fourth-order perturbation theory in the Hubbard model for $S \geq 1$ systems. In this model, Y is of the same order of magnitude as B and K, involving also two virtual excitations but spread over three sites (instead of two or four sites for B and K, respectively). With this additional interaction, the energy differences calculated in Refs. [10,24] are now expressed as (see also Fig. 1)

$$E_{2Q,\frac{\bar{M}}{2}} - E_{\frac{\bar{M}}{2}} = 4(2K_1 - B_1 - Y_1), \tag{3}$$

$$E_{2Q,\frac{3\bar{K}}{4}} - E_{\frac{3\bar{K}}{4}} = 4(2K_1 - B_1 + Y_1). \tag{4}$$

Here, $E_{2Q.q}$ is the energy of the $2Q$ state which results from the superpositions of $\pm q$ and E_q is the energy of the $1Q$ state. To fully specify the three higher-order interaction constants, we have to include the energy difference between a $3Q$ structure [25] and the constituting $1Q$ state (here, $q = \bar{M}$), to find

$$E_{3Q} - E_{\bar{M}} = \frac{16}{3}(2K_1 + B_1 - Y_1), \tag{5}$$

amounting to −2.5 meV/atom. Taking these three energy differences, we are now able to calculate the prefactors of the three interactions: $B_1 = 3.39$ meV, $Y_1 = 4.00$ meV, and $K_1 = 0.07$ meV. The value of Y_1 is not only on the same order of magnitude as the biquadratic interaction but also comparable with the nearest-neighbor exchange interaction ($J_1 = 3.8$ meV) [26]. Therefore, we argue that the ground state in Fe/Rh(111) is the result of the interplay between the biquadratic and a strong four-spin–three-site interaction.

In view of this additional interaction, we reanalyzed the parametrization of the magnetic energy landscape of Fe/Ir(111) [3] and found that the three-site interaction is small. Including the three-site interaction, the parametrization changes from $(B, K) = (-0.2, -1.05)$ meV to $(B, Y, K) = (-0.24, 0.24, -1.28)$ meV. This demonstrates that Y_1 is much smaller in this system; nevertheless, inclusion improves the fitting of the density-functional theory energy differences to the model Hamiltonian for the six magnetic structures listed in Ref. [3] (supplement) from $|\overline{\Delta E}| = 0.72$ meV to $|\overline{\Delta E}| = 0.24$ meV per Fe atom.

In summary, we found a $\uparrow\uparrow\downarrow\downarrow$ magnetic ground state of an Fe monolayer on Rh(111), which exists in three orientational domains. This exotic ground state discloses the existence of the three-site interaction. To the best of our knowledge, this is the first manifestation of this beyond-Heisenberg interaction in thin metallic films. Since the interaction is nonzero for atoms with spin $S \geq 1$, and many transition-metal atoms at interfaces experience a reduced coordination number which leads to enhanced magnetic moments, we expect quite generally that this interaction distinctly contributes to the spin coupling of many transition-metal atom triads in thin films. For example, for Fe/Ru(0001), a strong three-site term can be anticipated [26]. If Heisenberg interactions are not dominant, ground state properties will be influenced. More systematic research is necessary to identify under which circumstances a large three-site term can be expected. It would be interesting to material dependently control the strength of the different four-spin interactions such that nonchiral Skyrmions can be formed.

S. B. and G. B. thank Ali Al-Zubi for fruitful discussions. This work has been funded by King Saud University and by Deutsche Forschungsgemeinschaft (Project No. BO 1468/22-1).

Note added in proof—An very similar spin structure has recently been observed for Rh/Fe bilayers on Ir(111) [27].

[1] S. Mühlbauer, B. Binz, F. Jonietz, C. Pfleiderer, A. Rosch, A. Neubauer, R. Georgii, and P. Böni, Science **323**, 915 (2009).
[2] X. Yu, Y. Onose, N. Kanazawa, J. Park, J. H. Han, Y. Matsui, N. Nagaosa, and Y. Tokura, Nature (London) **465**, 901 (2010).
[3] S. Heinze, K. von Bergmann, M. Menzel, J. Brede, A. Kubetzka, R. Wiesendanger, G. Bihlmayer, and S. Blügel, Nat. Phys. **7**, 713 (2011).
[4] A. Fert, N. Reyren, and V. Cros, Nat. Rev. Mater. **2**, 17031 (2017).
[5] M. Takahashi, J. Phys. C **10**, 1289 (1977).
[6] A. H. MacDonald, S. M. Girvin, and D. Yoshioka, Phys. Rev. B **37**, 9753 (1988).
[7] A. Szilva, M. Costa, A. Bergman, L. Szunyogh, L. Nordström, and O. Eriksson, Phys. Rev. Lett. **111**, 127204 (2013).
[8] T. Skyrme, Proc. R. Soc. A **260**, 127 (1961).
[9] S.-Z. Lin and S. Hayami, Phys. Rev. B **93**, 064430 (2016).
[10] A. Al-Zubi, G. Bihlmayer, and S. Blügel, Phys. Status Solidi (b) **248**, 2242 (2011).
[11] D. D. Osheroff, M. C. Cross, and D. S. Fisher, Phys. Rev. Lett. **44**, 792 (1980).
[12] T. Soda, T. Arai, and K. Yoshida, Prog. Theor. Phys. **70**, 897 (1983).
[13] T. A. Kaplan, Phys. Rev. B **80**, 012407 (2009).
[14] M. Hoffmann and S. Blügel, arXiv:1803.01315.
[15] U. Falk, A. Furrer, H. U. Güdel, and J. K. Kjems, Phys. Rev. Lett. **56**, 1956 (1986).
[16] J. Kemmer, S. Wilfert, J. Kügel, T. Mauerer, P.-J. Hsu, and M. Bode, Phys. Rev. B **91**, 184412 (2015).
[17] P.-J. Hsu, J. Kügel, J. Kemmer, F. Parisen Toldin, T. Mauerer, M. Vogt, F. Assaad, and M. Bode, Nat. Commun. **7**, 10949 (2016).
[18] M. Bode, Rep. Prog. Phys. **66**, 523 (2003).
[19] P.-J. Hsu, A. Finco, L. Schmidt, A. Kubetzka, K. von Bergmann, and R. Wiesendanger, Phys. Rev. Lett. **116**, 017201 (2016).
[20] See Supplemental Material at http://link.aps.org/supplemental/10.1103/PhysRevLett.120.207202 for the full series of field-dependent SP-STM images, for in-plane sensitive SP-STM data, and for a discussion of field-induced changes to the antiferromagnetic spin structure, which includes Refs. [21–23].
[21] A. Kubetzka, O. Pietzsch, M. Bode, and R. Wiesendanger, Phys. Rev. B **67**, 020401 (2003).
[22] M. Bode, M. Heide, K. von Bergmann, P. Ferriani, S. Heinze, G. Bihlmayer, A. Kubetzka, O. Pietzsch, S. Blügel, and R. Wiesendanger, Nature (London) **447**, 190 (2007).
[23] M. Bode, E. Y. Vedmedenko, K. von Bergmann, A. Kubetzka, P. Ferriani, S. Heinze, and R. Wiesendanger, Nat. Mater. **5**, 477 (2006).
[24] A. Al-Zubi, *Ab Initio Investigations of Magnetic Properties of Ultrathin Transition Metal Films on 4d Substrates* (Forschungszentrum Jülich, Jülich, 2010), Vol. 16.
[25] P. Kurz, G. Bihlmayer, K. Hirai, and S. Blügel, Phys. Rev. Lett. **86**, 1106 (2001).
[26] B. Hardrat, A. Al-Zubi, P. Ferriani, S. Blügel, G. Bihlmayer, and S. Heinze, Phys. Rev. B **79**, 094411 (2009).
[27] N. Romming, H. Pralow, A. Kubetzka, M. Hoffmann, S. von Malottki, S. Meyer, B. Dupé, R. Wiesendanger, K. von Bergmann, and S. Heinze, preceding Letter, Phys. Rev. Lett. **120**, 207201 (2018).